ISSN 1070-3284, Russian Journal of Coordination Chemistry, 2024, Vol. 50, No. 7, pp. 523–533. © Pleiades Publishing, Ltd., 2024.

Imidazolium Salts with Heterometallic Complex Anions $[Co_2Li_2(Piv)_8]^{2-}$: Synthesis, Structures, and Magnetic Properties

I. K. Rubtsova[a], P. N. Vasilyev[a], J. K. Voronina[a], M. A. Shmelev[a], N. N. Efimov[a], S. A. Nikolaevskii[a, *], I. L. Eremenko[a], and M. A. Kiskin[a]

[a] *Kurnakov Institute of General and Inorganic Chemistry, Russian Academy of Sciences, Moscow, Russia*

**e-mail: sanikol@igic.ras.ru*

Received December 4, 2023; revised February 26, 2024; accepted February 27, 2024

Abstract—Imidazolium salts with complex anions $[Co_2Li_2(Piv)_8]^{2-}$ are formed as undesirable products of the reactions of heterometallic compound $[Co_2Li_2(Piv)_6(Py)_2]$ with N-heterocyclic carbenes ItBu and IPr. The study of the magnetic properties of complex $(HItBu)_2[Co_2Li_2(\mu^2\text{-}Piv)_6(\kappa^1\text{-}Piv)_2]$ shows that this compound is a single molecule magnet. Slow magnetic relaxation in the complex occurs due to a combination of the direct and Raman mechanisms.

Keywords: carboxylate ligands, heterometallic complexes, cobalt(II), lithium(I), molecular structure, magnetic properties

DOI: 10.1134/S1070328424600256

INTRODUCTION

The use of carboxylic acid anions as ligands is an important tool for the solution of a broad range of problems of the chemistry of coordination compounds: from the development of fundamental principles of crystalline packing engineering due to noncovalent interactions [1–8] to the preparation of prototypes of materials with photoluminescence [9–15], magnetic [16], catalytic [17–21], and other functional properties [22–24].

A particular area of coordination chemistry, which is mainly developed due to the application of carboxylate ligands, is the chemistry of heterometallic complexes [25–27]. Molecular complexes based on Co(II) and lithium(I) cations should be noted among diverse classes of heterometallic carboxylate complexes [28]. These compounds are considered as precursors of materials for lithium-ion batteries [29, 30], prototypes of extracting agents for selective binding Cs^{137} cations [31], and secondary building units for the formation of heterometallic metal-organic frameworks with a broad range of practically useful properties [32–37].

The cobalt(II) carboxylate complexes are actively studied as single molecule magnets (SMM) [38] and single ion magnets (SIM) [39–41]. A common drawback of the SMM and SIM based on the Co(II) carboxylate complexes is their tendency to manifest magnetic anisotropy of the "easy-plane" type and slow magnetization relaxation via the direct and Raman mechanisms [39–42], whereas anisotropy of the "easy-axis" type and relaxation via the Orbach mechanism are preferred for the design of functional materials [43, 44]. The strategy that makes it possible to switch over the "easy-plane" anisotropy and "easy-axis" anisotropy by the dilution of the paramagnetic congener of cobalt(II) pivalate with a close in structure diamagnetic analog based on zinc(II) pivalate was proposed [45]. An alternative strategy is the organization of diamagnetic dilution at the molecular level due to the introduction of alkaline and alkaline-earth metals, which play an important structure forming role, into the cobalt(II) carboxylate complexes [46–49].

We are performing a systematic research on the synthesis and studies of the properties of transition metal carboxylate complexes with N-heterocyclic carbenes (NHC) [50–55]. These objects were unknown before the publication of our works [56]. It has recently been shown that the $[Co_2Li_2(Piv)_6(IMes)_2]$ complex (Piv is pivalate anion, and IMes is 1,3-bis(2,4,6-trimethylphenyl)imidazol-2-ylidene) is SMM, the slow magnetization relaxation in which is described by the sum of the Raman and direct processes [48]. It was of interest to extend the series of these compounds by the synthesis of similar derivatives with carbenes I*t*Bu (1,3-di-*tert*-butylimidazol-2-ylidene) and IPr (1,3-bis(2,6-diisopropylphenyl)imidazol-2-ylidene). However, the attempts to synthesize these compounds with ligands of the NHC family resulted in the isolation of compounds of the protonated forms of these ligands with the $[Co_2Li_2(Piv)_8]^{2-}$ complex anions.

EXPERIMENTAL

All procedures associated with the synthesis of the coordination compounds were carried out in an inert atmosphere using evacuated glass tubes. Dehydrated solvents were used for the synthesis. Tetrahydrofuran (THF) was stored over the sodium complex with benzophenone, and hexane was stored over "sodium mirror" and transferred by vacuum condensation prior to synthesis. Complex $[Co_2Li_2(Piv)_6(Py)_2]$ and NHC were synthesized using known procedures [34, 57].

The IR spectra of the compounds were recorded in a range of 400–4000 cm^{-1} on a Perkin Elmer Spectrum 65 spectrophotometer equipped with a Quest ATR Accessory instrument (Specac) using the attenuated total internal reflectance (ATR) mode. Elemental analysis was conducted on a Euro EA-3000(EuroVector) automated C,H,N,S analyzer.

The magnetic susceptibility was measured on a Quantum Design PPMS-9 automated complex for physical measurements with the option for measuring magnetic properties. This equipment makes it possible to measure the magnetic properties in the temperature range from 1.8 to 300 K in the external magnetic fields up to 9 T. An alternating magnetic field with an intensity of 1, 3, and 5 Oe in frequency ranges of 10000–1000, 1000–100, 100–10 Hz, respectively, was used for measuring the dynamic magnetic susceptibility. These settings make it possible to both avoid sample heating at low temperatures (which can take place at high modulation amplitudes and frequencies) and obtain the best signal/noise ratio. The dynamic magnetic susceptibility was measured and the results were processed using a standard procedure [58]. The measurements were performed on polycrystalline samples preliminarily mixed with mineral oil and sealed in polyethylene bags to prevent the orientation of crystallites under the external magnetic field. The paramagnetic component of the magnetic susceptibility (χ) was determined with account for the diamagnetic contribution of the sample estimated by the additive Pascal equation, as well as the contributions of the sample holder and mineral oil.

Synthesis of $(HI\mathit{t}Bu)_2[Co_2Li_2(\mu^2\text{-}Piv)_6(\kappa^1\text{-}Piv)_2]\cdot 0.67THF$ (I). THF was added by vacuum condensation to a weighed sample of complex $[Co_2Li_2(Piv)_6(Py)_2]$ (0.09 g, 0.1 mmol) preliminarily evacuated in a glass tube. A minor amount of THF was condensed from the tube with a solution of the complex to a tube with a weighed sample of I*t*Bu (0.036 g, 0.2 mmol), which was preliminarily weighed in a glove box. After the carbene was dissolved, the resulting solution was poured to a solution of the complex, and the reaction mixture was boiled. Then THF was completely removed by vacuum condensation to get rid of pyridine. Hexane and a minimum amount of THF necessary for the dissolution of the precipitate were added by vacuum condensation, and the reaction mixture was boiled. The resulting solution was concentrated under reduced pressure to form crimson single crystals suitable for XRD. The yield was 0.048 g (35% based on the initial heterometallic complex).

For $C_{64.68}H_{119.36}N_4O_{16.66}Li_2Co_2$			
Anal. calcd., %	C, 57.38	H, 8.82	N, 4.12
Found, %	C, 57.15	H, 8.78	N, 4.10

IR (ν, cm^{-1}): 3127 w, 2958 s, 2925 s, 2867 m, 1597 vs, 1564 vs, 1480 vs, 1413 vs, 1359 vs, 1292 w, 1212 vs, 1124 s, 1071 w, 1031 w, 891 s, 793 s, 752 m, 658 m, 605 vs, 563 m, 417 vs.

Synthesis of $(HIPr)_2[Co_2Li_2(\mu^2\text{-}Piv)_6(\kappa^1\text{-}Piv)_2]\cdot 3THF$ (II). THF was added by vacuum condensation to a weighed sample of complex $[Co_2Li_2(Piv)_6(Py)_2]$ (0.09 g, 0.1 mmol) in a preliminarily evacuated glass tube. A minor amount of THF was condensed from the tube with a solution of the complex to a tube with a weighed sample of IPr (0.077 g, 0.2 mmol), which was preliminarily weighed in a glove box. After the carbene was dissolved, the resulting solution was poured to a solution of the complex, and the reaction mixture was boiled. Then THF was completely removed by vacuum condensation to get rid of pyridine. Hexane and a minimum amount of THF necessary for the dissolution of the precipitate were added by vacuum condensation, and the reaction mixture was boiled. The obtained solution was concentrated under reduced pressure to form violet single crystals suitable for XRD. The yield was 0.012 g (6% based on the initial heterometallic complex).

For $C_{106}H_{170}N_4O_{19}Li_2Co_2$			
Anal. calcd., %	C, 65.75	H, 8.85	N, 2.89
Found, %	C, 65.48	H, 8.81	N, 2.87

IR (ν, cm^{-1}): 3069 w, 2963 vs, 2925 s, 2872 s, 1595 vs, 1562 vs, 1480 vs, 1408 vs, 1357 vs, 1222 vs, 1106 m, 1062 s, 1033 w, 935 m, 894 s, 796 vs, 757 s, 684 s, 607 vs, 568 s, 435 vs.

XRD of single crystals of complexes **I** and **II** was conducted on a Bruker D8 Venture diffractometer equipped with a CCD detector and a monochromatic radiation source (MoK_α, λ = 0.71073 Å, graphite monochromator) using standard procedures [59]. A semiempirical absorption correction was applied for both structures [60, 61]. The structures were solved by a direct method and refined in the full-matrix anisotropic approximation for all non-hydrogen atoms. The structures were refined using the DFIX, ISOR, RIGU, and SADI standard restraints taking into account the partial disordering of the $CHMe_2$ and CMe groups and THF molecules. The calculations were performed using the SHELX-2018/3 [62, 63] and Olex2 [64] programs. The geometry of the metal atom polyhedra was determined using the SHAPE 2.1 pro-

Table 1. Crystallographic parameters and structure refinement details for compounds **I** and **II**

Parameter	Value	
	I	**II**
Empirical formula	$C_{64.68}H_{119.36}N_4O_{16.66}Li_2Co_2$	$C_{106}H_{170}N_4O_{19}Li_2Co_2$
FW, g/mol	1351.53	1936.19
T, K	100(2)	100(2)
Space group; *Z*	$P2_1/n$; 2	$P2_1/c$; 2
a, Å	12.5864(7)	22.118(3)
b, Å	17.2898(13)	11.2825(15)
c, Å	17.6946(12)	23.611(3)
β, deg	95.292(2)	112.141(3)
V, Å^3	3834.2(4)	5457.5(13)
ρ_{calc}, g/cm^3	1.171	1.178
μ, mm^{-1}	0.494	0.368
θ, deg	1.91–26.00	1.99–30.57
Ranges of indices *h*, *k*, *l*	$-15 \le h \le 15$, $-21 \le k \le 21$, $-21 \le l \le 21$	$-27 \le h \le 31$, $-12 \le k \le 16$, $-33 \le l \le 33$
Number of reflections: measured/independent	30410, 7500	60970, 16715
Number of observed reflections with $I \ge 2\sigma(I)$/refined parameters	3227/451	10362/717
R_{int}	0.1914	0.0682
T_{min}/T_{max}	0.3027/0.3812	0.3408/0.3812
S	0.956	1.030
R_1, wR_2 ($I \ge 2\sigma(I)$)	0.0806, 0.1316	0.0661, 0.1579
R_1, wR_2 (all values)	0.2109, 0.1316	0.1194, 0.1854
$\Delta\rho_{min}/\Delta\rho_{max}$, e/Å^3	−0.072/0.622	−0.590/0.704

gram [65]. The crystallographic parameters and structure refinement details are given in Table 1.

The coordinates of atoms, thermal parameters, and all reflections were deposited with the Cambridge Crystallographic Data Centre (CIF files CCDC nos. 2311574 (**I**) and 2311575 (**II**); deposit@ccdc.cam.ac.uk or http://www.ccdc.cam.ac.uk/structures).

The powder XRD pattern of complex **I** was detected on a Bruker D8 Advance X-ray diffractometer equipped with a Ni monochromator ($\lambda(CuK_{\alpha 1})$ = 1.54060 Å) and a LynxEye position-sensitive detector. The detection increment was 0.02° 2θ, and the detection range was 5°–40° 2θ. The PXRD pattern (Fig. 1) was simulated in the TOPAS 4 program. The unit cell parameters were optimized in refinement, the effects of predominant crystallite orientation were described

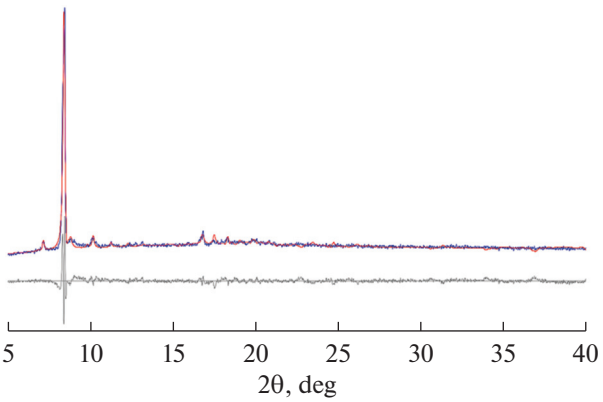

Fig. 1. Theoretical (red line) and experimental (blue line) PXRD patterns of complex **I** and their difference (gray line).

by spherical fourfold harmonics, and the line broadening was refined by the Williamson–Hall method.

RESULTS AND DISCUSSION

Anionic carboxylate complexes are met in the literature rather rarely. A significant part of these compounds was published fairly long ago [66–71]. The $(HI\mathit{t}Bu)_2[Co_2Li_2(\mu^2\text{-}Piv)_6(\kappa^1\text{-}Piv)_2]$ (**I**) and $(HIPr)_2[Co_2Li_2(\mu^2\text{-}Piv)_6(\kappa^1\text{-}Piv)_2]$ (**II**) complexes were synthesized by the reactions of the earlier prepared compound $[Co_2Li_2(Piv)_6(Py)_2]$ with two equivalents of NHC (Scheme 1).

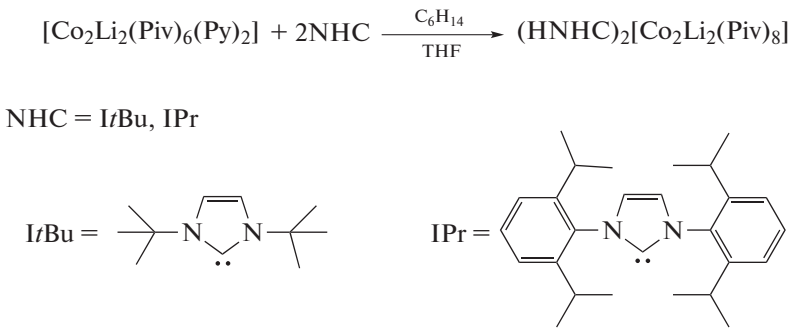

Scheme 1.

Compounds **I** and **II** crystallize in the monoclinic crystal systems with space groups $P2_1/n$ and $P2_1/c$, respectively, and represent ionic complexes consisting of the dianionic fragment $[Li_2Co_2(Piv)_8]^{2-}$, two $[HNHC]^+$ cations, and solvate THF molecules. In both complexes, the dianionic $[Li_2Co_2(Piv)_8]^{2-}$ fragment is centrosymmetric, and the inversion center is localized between two central Li(1) atoms. The Co(1) and Li(1) atoms are bound by three bridging carboxylate groups, one of which performs an additional bridging function linking two lithium atoms by one oxygen atom (Fig. 2, selected bond lengths and angles are given in Table 2). The central Li_2O_2 fragment corresponds to a distorted square (Li(1)–O(7) 1.938(9), 2.022(10) Å, Li(1)O(7)Li(1) 89.5(4)°, O(7)Li(1)O(7) 90.5(4)° for **I**; Li(1)–O(4) 1.968(4), 1.979(4) Å, Li(1)O(4)Li(1) 89.77(17)°, O(4)Li(1)O(4) 90.22(17)° for **II**). The coordination environment of the cobalt atoms surrounded by four atoms of the carboxylate anions corresponds to a distorted tetrahedron in complex **II** ($S_Q = 0.883$) and a more distorted tetrahedron in compound **I** ($S_Q = 2.918$). This distortion is caused by the orientation of the fourth monodentate-coordinated carboxylate group: in complex **I**, the orientation is close to the chelate one (Fig. 2a; Co(1)...O(6) 2.560 Å, Co(1)O(5)O(6) angle 74.73°); in complex **II**, the group is directed along the Li(1)Co(1)O(7) vector (Fig. 2b; Co(1)...O(8) 4.113 Å, Co(1)O(5)O(6) angle 167.27°). Contacts C–H...O are formed between the oxygen atoms of the carboxylate groups in $[Li_2Co_2(Piv)_8]^{2-}$ and the imidazole fragment protons of the outer-sphere organic cation: in **I**: two vicinal protons are involved in interactions with the O(4) and O(6) atoms of one $[Li_2Co_2(Piv)_8]^{2-}$ fragment and the proton at the C(21) atom interacts with the O(5) atom of another $[Li_2Co_2(Piv)_8]^{2-}$ fragment (Fig. 3, Table 3); in **II**: two vicinal protons form hydrogen bonds with the O(1) and O(8) atoms and the proton at the C(21) atom forms a hydrogen bond with the O(1S) atom of the solvate THF molecule (Fig. 4, Table 3). In complex **I**, the hydrogen atoms of the *tert*-butyl groups of the $HI\mathit{t}Bu^+$ cation also participate in intermolecular contacts with the oxygen atoms of the solvate THF molecules.

The crystal of complex **II** exhibits intermolecular C–H...O contacts between the protons of the phenyl fragments (C(26), C(40)) of the $HIPr^+$ cations with the oxygen atoms of the carboxylate groups (Table 3) and C–H...π contacts between the protons of the methyl group in $HIPr^+$ (C(46)/C(46A)) and the phenyl cycle of the adjacent $HIPr^+$ cation (Table 4). Thus, the intermolecular noncovalent binding of the $[Li_2Co_2(Piv)_8]^{2-}$ anions and $[HNHC]^+$ cations leads to the formation of layered supramolecular structures.

The magnetic susceptibility in a direct current field of complex **I** was measured at a magnetic field intensity of 5000 Oe in a temperature range of 2–300 K to determine magnetochemical purity (Fig. 5). At 300 K χT = 5.77 cm^3 K mol^{-1}, which is substantially higher than the spin-only values for two noninteracting cobalt(II) ions (3.79 cm^3 K mol^{-1}, $^4F_{9/2}$, $S = 3/2$, $L = 3$) [72, 73]. This can be explained by a considerable orbital contribution. As the temperature decreases, the values of χT decrease smoothly, and the slope of the $\chi T(T)$ dependence increases appreciably when 40 K was reached. The minimum value of χT equal to 2.51 cm^3 K mol^{-1} is achieved at 2 K. This magnetic behavior is related, most probably, to a significant magnetic anisotropy or to the Zeeman effect (saturation) in the magnetic field [43].

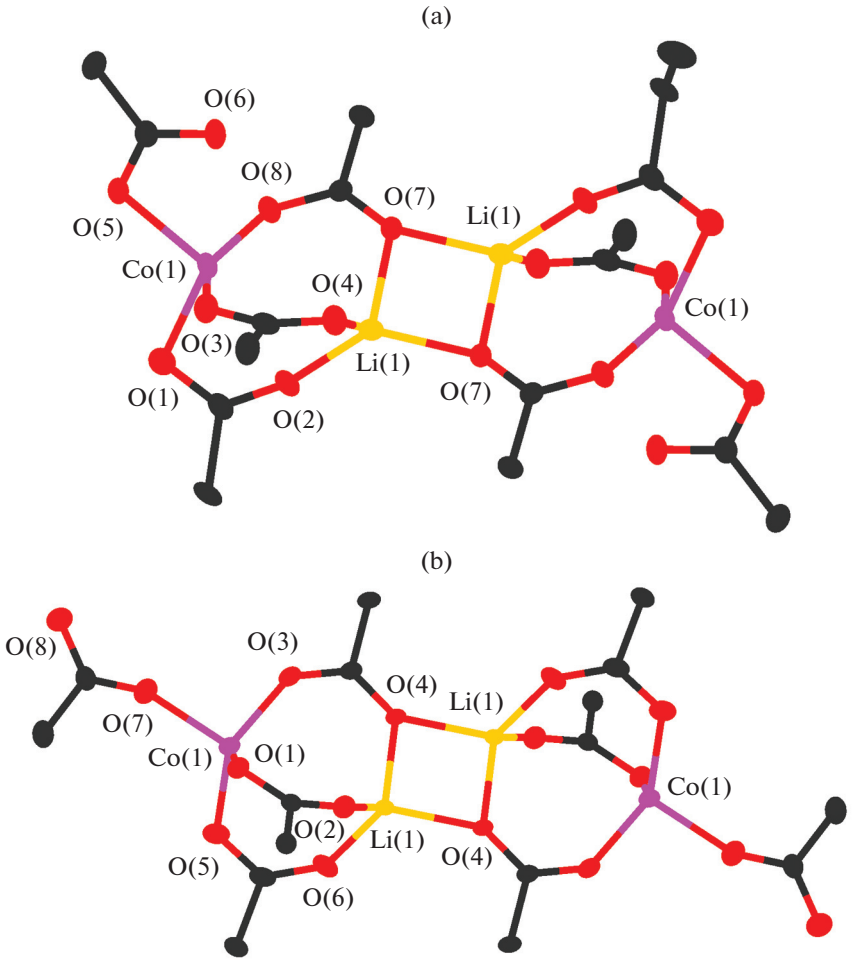

Fig. 2. Structures of dianions $[Li_2Co_2(Piv)_8]^{2-}$ in complexes (a) **I** and (b) **II** (thermal ellipsoids with 30% probability; methyl groups are omitted).

The data on measurements of the temperature dependences of the static magnetic susceptibility and the field dependences of the magnetization of compound **I** are presented in Figs. 5 and 6, respectively.

The experimental $\chi T(T)$ and $M(H)$ dependences were approximated using the PHI program according to the spin-Hamiltonian (SH) [74]:

$$\hat{H} = g\mu_B HS + D\left[\hat{S}_z^2 - \frac{1}{3}S(S+1)\right] + E\left(\hat{S}_x^2 - \hat{S}_y^2\right) - 2S_1J_{12}S_2,$$

where μ_B is the Bohr magneton, H is the magnetic field intensity, S is the total spin, D and E are the splitting parameters in the zero field, $\hat{S}$ is the spin operator, and J_{12} is the exchange interaction parameter.

The best approximation of the experimental data was achieved at the following SH parameters: $g = 2.3$, $D = 5.05$ cm^{-1}, $E/D = 1.5$, $J_{12} = -0.054$, and $\chi_{TIP} = 2.2 \times 10^{-3}$ ($R^2 = 1.2 \times 10^{-2}$).

The dynamic magnetic susceptibility was studied to determine whether complex **I** had slow magnetic relaxation. The frequency dependences of the imaginary part of the dynamic magnetic susceptibility $\chi''(\nu)$ of complex **I** in the zero magnetic field show signals negligible compared to the real part. The application of direct current magnetic field H_{DC} results in the appearance of significant signals on the $\chi''(\nu)$ dependences, which indicates the contribution of the effect of quantum tunneling of magnetization (QTM) to the relaxation. The variation of H_{DC} made it possible to determine the optimum magnetic field (500 Oe), the application of which resulted in the arrangement of the maxima on the respective dependences $\chi''(\nu)$ at the lowest frequencies corresponding to the longest relaxation times.

The isotherms of the frequency dependences of the dynamic magnetic susceptibility were measured in a temperature range of 2–2.75 K to determine the temperature dependence of the relaxation time in the optimum magnetic field (Fig. 7). The magnetization relaxation times were determined by the approxima-

Table 2. Selected bond lengths, distances between the central atoms (Å), and angles (deg) in complexes **I** and **II**

Bond	**I**	**II**
	d, Å	
Co–O	1.966(3)–2.050(4)	1.9401(19)–1.9651(17)
Li–O	1.902(9)–2.022(10)	1.906(4)–1.979(4)
C–O	1.255(6)–1.281(5)	1.238(3)–1.277(3)
C–N(Pz)	1.328(7)–1.381(7)	1.326(3)–1.379(3)
N–C(Ph; CMe_3)	1.479(7), 1.501(7)	1.449(3), 1.455(3)
Li...Li	2.789(18)	2.785(8)
Co...Li	3.043(9)	3.241(4)
Angle	ω, deg	
OCoO	96.50(15)–145.23(15)	96.08(8)–119.62(8)
OLiO	90.5(4)–127.5(5)	90.22(17)–121.8(2)
CoLiLi	122.5(5)	123.6(2)
OCO	121.3(5)–124.9(5)	122.7(3)–125.1(2)

tion of the dependences of the imaginary part of the dynamic magnetic susceptibility on the frequency using the generalized Debye model. These data were used to deduce the dependences of the relaxation time on the inverse temperature $\tau(1/T)$ for complex **I** (Fig. 8).

The $\tau(1/T)$ dependence of complex **I** deviates appreciably from linearity in the semilogarithmic

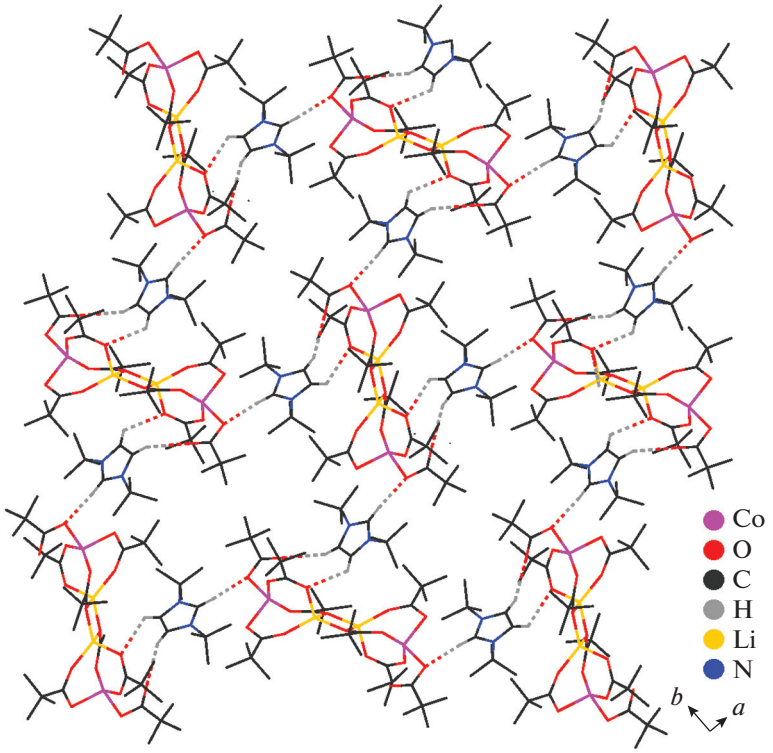

Fig. 3. Fragment of the packing of complex **I** (intermolecular interactions C–H...O are shown by dashed lines; solvate molecules and hydrogen atoms at the methyl groups are omitted).

Table 3. Geometric parameters of hydrogen bonds in complexes **I** and **II**

C–H...O	Distance, Å			Angle C–H...O, deg
	C–H	H...O	C...O	
I				
C(19)–H(19A)...O(4)	0.98	2.57	3.502(8)	160
C(21)–H(21)...O(5)	0.95	2.23	3.178(7)	174
C(22)–H(22)...O(4) $1/2 + x$, $3/2 - y$, $1/2 + z$	0.95	2.43	3.061(7)	123
C(23)–H(23)...O(6) $1/2 + x$, $3/2 - y$, $1/2 + z$	0.95	2.59	3.499(7)	159
C(27)–H(27C)...O(1S) $3/2 - x$, $1/2 + y$, $3/2 - z$	0.98	2.51	3.43(2)	156
C(29)–H(29C)...O(1S)	0.98	2.36	3.32(2)	167
II				
C(21)–H(21)...O(1S) x, $1/2 - y$, $1/2 + z$	0.95	2.12	3.014(4)	157
C(22)–H(22)...O(1)	0.95	2.24	3.179(3)	170
C(23)–H(23)...O(8)	0.95	2.18	3.084(3)	158
C(26)–H(26)...O(5) x, $-1 + y$, z	0.95	2.57	3.426(3)	151
C(40)–H(40)...O(8) $1 - x$, $-1/2 + y$, $3/2 - z$	0.95	2.37	3.214(3)	148
C(46*A*)–H(46B)...O(8) $1 - x$, $-1/2 + y$, $3/2 - z$	0.98	2.57	3.538(5)	168

Table 4. Interactions C–H...π in the crystalline packing of complex **II** (Cg_i centroid phenyl cycle; H/C...Cg is the distance from the centroid to the atom, H–Perp is the shortest distance from the H atom to the cycle plane, γ is the angle between the Cg_i–H vector and normal to the *i*th plane, C–H...Cg angle)

Interaction	H...Cg, Å	H–Perp, Å	γ, deg	C–H...Cg, deg	C...Cg, Å
C(42)–H(42A)...Cg(N(1)C(21)N(2)C(23)C(22))	2.99	2.32	39.02	119	3.578(3)
C(45)–H(45)...Cg(N(1)C(21)N(2)C(23)C(22))	2.89	2.48	31.17	125	3.564(3)
C(46A)–H(46A)...Cg(C(36)–C(41)) $1 - x$, $-1/2 + y$, $3/2 - z$	2.9	2.84	11.94	137	3.686(6)
C(42)–H(42)...Cg(N(1)C(21)N(2)C(23)C(22))	2.92(7)	2.32	37.35	132(6)	3.578(3)
C(46)–H(46E)...Cg(C(36)–C(41)) $1 - x$, $-1/2 + y$, $3/2 - z$	2.9	2.85	9.94	135	3.658(16)

system of coordinates (Fig. 8). In order to compare complex **I** with similar compounds, the high-temperature part of the relaxation time dependence was approximated by the Arrhenius equation ($\tau = \tau_0 \exp\{\Delta E/k_B T\}$), which made it possible to estimate the effective energy barrier equal to 19 K and the fastest relaxation time in the system equal to 2.2×10^{-9} s. The approximation of the $\tau(1/T)$ dependence of complex **I** by the sum of the direct ($\tau^{-1} = A_{direct} H^{n\_direct} T$) and Raman ($\tau^{-1} = C_{Raman} T^{n\_Raman}$) relaxation mechanisms resulted in a satisfactory correspondence of the experimental and theoretical curves at the following parameters: $A_{direct} = 1.82 \times 10^{-8} \pm 4.32 \times 10^{-10}$ s^{-1} $Oe^{-\ n\_direct}$, $n_{direct} = 4$, $C_{Raman} = 4.76 \pm 0.09$ s^{-1} $K^{-nRaman}$, and $n_{Raman} = 9$ ($R^2 = 0.9999$).

Thus, the imidazolium salts with the $[Co_2Li_2(Piv)_8]^{2-}$ complex anions were formed as undesirable products of the reactions of the heterometallic compound $[Co_2Li_2(Piv)_6(Py)_2]$ with *N*-heterocyclic carbenes I*t*Bu and IPr. The satisfactory yield of compound $(HI{t}Bu)_2[Co_2Li_2(\mu^2\text{-}Piv)_6(\kappa^1\text{-}Piv)_2]$ (**I**) made it possible to confirm its phase purity by PXRD and to study its magnetic properties. Complex **I** is a single molecule magnet. The magnetic relaxation of this compound proceeds via the cumulative contribution of the direct and Raman relaxation mechanisms.

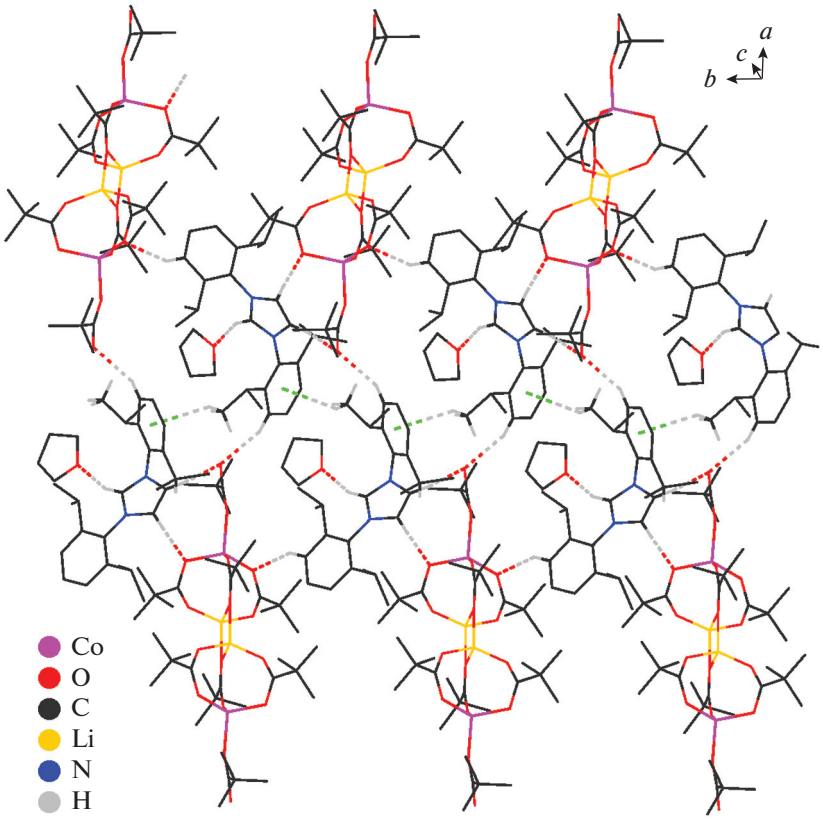

Fig. 4. Fragment of the packing of complex **II** (intermolecular interactions C–H...O and C–H...π are shown by dashed lines; hydrogen atoms that are not involved in intermolecular interactions are omitted).

In the previously studied complexes $[Co_2Li_2(Piv)_6(IMes)_2]$, $[Co_2Li_2(Piv)_6(Ph_3P)_2]$, $[Co_2Li_2(Fur)_6(Py)_2]$ (Fur is 2-furancarboxylic acid anion) and $[Co_2Li_2(Piv)_6(4\text{-}MeOC_6H_4\text{-}MIAN)_2]$ (4-$MeOC_6H_4$-MIAN is *N*-(4-methoxyphenyl)monoiminoacenaphthenone), slow magnetization relaxation was also caused by a combination of the direct and Raman processes [48, 49]. The magnetization relaxation time

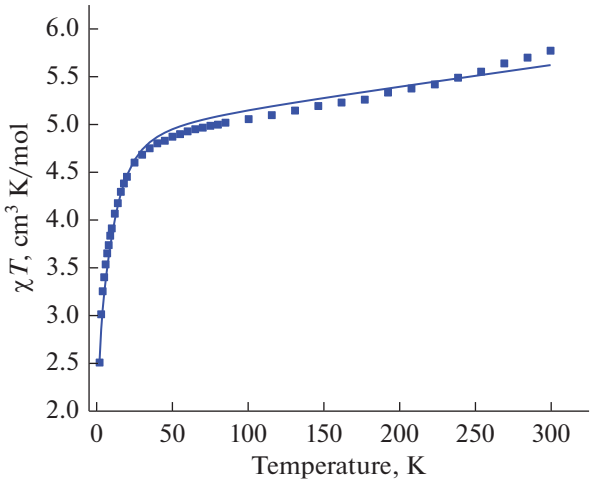

Fig. 5. Temperature dependence χT of complex **I** ($H = 5$ kOe). Solid line is the curve calculated using the PHI program.

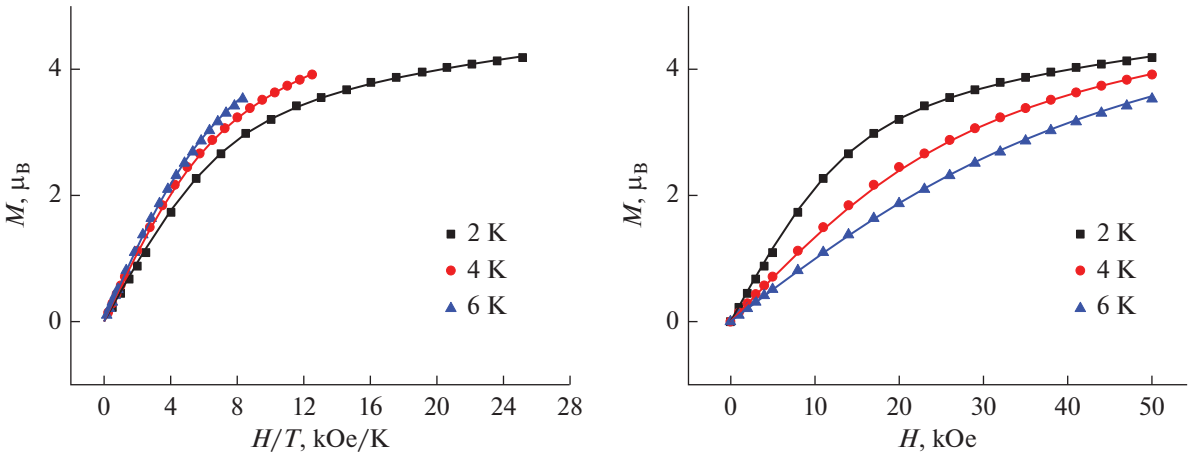

Fig. 6. Dependences $M(H/T)$ (left) and $M(H)$ (right) at various temperatures for complex **I**. Solid lines are the theoretical curves calculated using the PHI program.

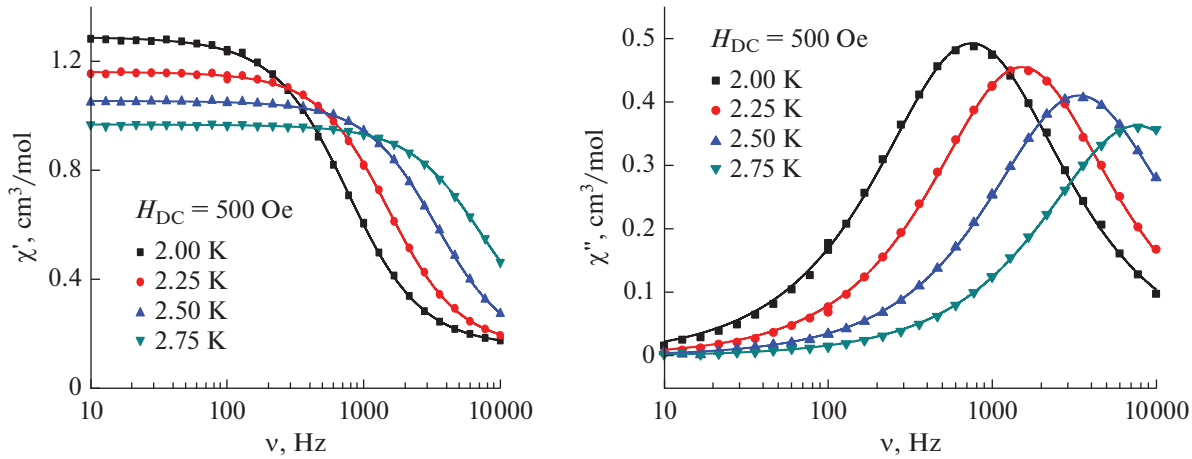

Fig. 7. Frequency dependences of the real (left) and imaginary (right) parts of the dynamic magnetic susceptibility of complex **I** at various temperatures; external magnetic field intensity H = 500 Oe. The approximation by the generalized Debye model is shown by solid lines.

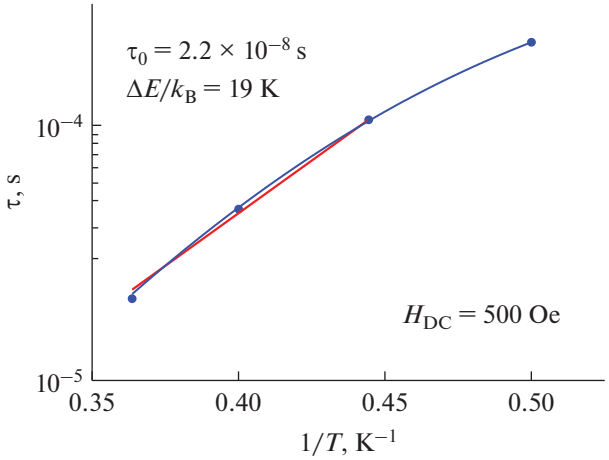

Fig. 8. Relaxation time as a function of inverse temperature $\tau(1/T)$ for complex **I**. Red line is the approximation of the high-temperature part (2.25–2.75 K) by the Arrhenius equation. Blue line is the approximation by the sum of the Raman and direct mechanisms.

increases more than twofold at 2 K on going from the neutral complex $[Co_2Li_2(Piv)_6(IMes)_2]$ [48] to the salt of the $[Co_2Li_2(Piv)_8]^{2-}$ complex anion (complex **I**), which can be due to the charge on the terminal ligand.

FUNDING

This work was supported by the Russian Science Foundation, project no. 19-13-00436-P.

CONFLICT OF INTEREST

The authors of this work declare that they have no conflicts of interest.

REFERENCES

1. Bondarenko, M.A., Rakhmanova, M.I., Plyusnin, P.E., et al., *Polyhedron*, 2021, vol. 194, p. 114895.

2. Vershinin, M.A., Rakhmanova, M.I., Novikov, A.S., et al., *Molecules*, 2021, vol. 26, no. 11, p. 3393.
3. Shmelev, M.A., Kuznetsova, G.N., Dolgushin, F.M., et al., *Russ. J. Coord. Chem.*, 2021, vol. 47, no. 2, p. 127. https://doi.org/10.1134/S1070328421020068
4. Bondarenko, M.A. and Adonin, S.A., *J. Struct. Chem.*, 2021, vol. 62, no. 8, p. 1251.
5. Bondarenko, M.A., Novikov, A.S., and Adonin, S.A., *Russ. J. Inorg. Chem.*, 2021, vol. 66, no. 6, p. 814.
6. Bondarenko, M.A., Abramov, P.A., Novikov, A.S., et al., *Polyhedron*, 2022, vol. 214, p. 115644.
7. Zaguzin, A.S., Sukhikh, T.S., Sakhapov, I.F., et al., *Molecules*, 2022, vol. 27, no. 4, p. 1305.
8. Zaguzin, A.S., Sukhikh, T.S., Kolesov, B.A., et al., *Polyhedron*, 2022, vol. 212, p. 115587.
9. Shmelev, M.A., Gogoleva, N.V., Ivanov, V.K., et al., *Russ. J. Coord. Chem.*, 2022, vol. 48, no. 9, p. 539. https://doi.org/10.1134/S1070328422090056
10. Goldberg, A., Kiskin, M., Shalygina, O., et al., *Chem. Asian J.*, 2016, vol. 11, no. 4, p. 604.
11. Kiraev, S.R., Nikolaevskii, S.A., Kiskin, M.A., et al., *Inorg. Chim. Acta*, 2018, vol. 477, p. 15.
12. Melnikov, S.N., Evstifeev, I.S., Nikolaevskii, S.A., et al., *New J. Chem.*, 2021, vol. 45, no. 30, p. 13349.
13. Utochnikova, V.V., Kalyakina, A.S., Lepnev, L.S., et al., *J. Lumin.*, 2016, vol. 170, p. 633.
14. Koshelev, D.S., Chikineva, T.Yu., Kozhevnikova (Khudoleeva), V.Yu., et al., *Dyes and Pigments*, 2019, vol. 170, p. 107604.
15. Utochnikova, V.V., Abramovich, M.S., Latipov, E.V., et al., *J. Lumin.*, 2019, vol. 205, p. 429.
16. Kottsov, S.Yu., Shmelev, M.A., Baranchikov A.E., et al., *Molecules*, 2023, vol. 28, no. 1, p. 418.
17. Akintayo, D.C., Munzeiwa, W.A., Jonnalagadda, S.B., and Omondi, B., *Polyhedron*, 2022, vol. 213, p. 115589.
18. Akintayo, D.C., Munzeiwa, W.A., Jonnalagadda, S.B., and Omondi, B., *Inorg. Chim. Acta*, 2022, vol. 532, p. 120715.
19. Takeuchi, K., Chen, M.-Y., Yuan, H.-Y., et al., *Chem.-Eur. J.*, 2021, vol. 27, no. 72, p. 18066.
20. Cheng, X., Liu, X., Wang, S., et al., *Nat. Commun.*, 2021, vol. 12, no. 1, p. 4366.
21. Hayashi, Y., Santoro, S., Azuma, Y., et al., *J. Am. Chem. Soc.*, 2013, vol. 135, no. 16, p. 6192.
22. Smith, R.M.S., Amiri, M., Martin, N.P., et al., *Inorg. Chem.*, 2022, vol. 61, no. 3, p. 1275.
23. Gusev, A., Baluda, Yu., Braga, E., et al., *Inorg. Chim. Acta*, 2021, vol. 528, p. 120606.
24. Lutsenko, I.A., Baravikov, D.E., Kiskin, M.A., et al., *Russ. J. Coord. Chem.*, 2020, vol. 46, no. 6, p. 411. https://doi.org/10.1134/S1070328420060056
25. Bazhina, E.S., Gogoleva, N.V., Zorina-Tikhonova, E.N., et al., *J. Struct. Chem.*, 2019, vol. 60, no. 6, p. 855.
26. Sidorov, A.A., Kiskin, M.A., Aleksandrov, G.G., et al., *Russ. J. Coord. Chem.*, 2016, vol. 42, no. 10, p. 621. https://doi.org/10.1134/S1070328416100031
27. Sidorov, A.A., Gogoleva, N.V., Bazhina, E.S., et al., *Pure Appl. Chem.*, 2020, vol. 92, no. 7, p. 1093.
28. Rubtsova, I.K., Nikolaevskii, S.A., Eremenko, I.L., and Kiskin, M.A., *Russ. J. Coord. Chem.*, 2023, vol. 49, no. 11, p. 695. https://doi.org/10.1134/S1070328423600766
29. Huang, P.-B., Tian, L.-Y., Zhang, Y.-H., and Shi, F.-N., *Inorg. Chim. Acta*, 2021, vol. 525, p. 120473.
30. Du, Z.-Q., Li, Y.-P., Wang, X.-X., et al., *Dalton Trans.*, 2019, vol. 48, no. 6, p. 2013.
31. Tian, D., Wu, T.-T., Liu, Y.-Q., and Li, N., *Inorg. Chem.*, 2021, vol. 60, no. 16, p. 12067.
32. Sapianik, A.A., Lutsenko, I.A., Kiskin, M.A., et al., *Russ. Chem. Bull.*, 2016, vol. 65, no. 11, p. 2601.
33. Sapianik, A.A. and Fedin, V.P., *Russ. J. Coord. Chem.*, 2020, vol. 46, no. 7, p. 443. https://doi.org/10.1134/S1070328420060093
34. Sapianik, A.A., Kiskin, M.A., Kovalenko, K.A., et al., *Dalton Trans.*, 2019, vol. 48, no. 11, p. 3676.
35. Dybtsev, D.N., Sapianik, A.A., and Fedin, V.P., *Mendeleev Commun.*, 2017, vol. 27, no. 4, p. 321.
36. Sapianik, A.A., Zorina-Tikhonova, E.N., Kiskin, M.A., et al., *Inorg. Chem.*, 2017, vol. 56, no. 3, p. 1599.
37. Li, Y.-P., Wang, X.-X., Li, S.-N., et al., *Cryst. Growth Des.*, 2017, vol. 17, no. 11, p. 5634.
38. Murrie, M., *Chem. Soc. Rev.*, 2010, vol. 39, no. 6, p. 1986.
39. Zorina-Tikhonova, E., Matyukhina, A., Skabitskiy, I., et al., *Crystals*, 2020, vol. 10, no. 12, p. 1130.
40. Yambulatov, D.S., Nikolaevskii, S.A., Kiskin, M.A., et al., *Molecules*, 2020, vol. 25, no. 9, p. 2054.
41. Yambulatov, D.S., Voronina, J.K., Goloveshkin, A.S., et al., *Int. J. Mol. Sci.*, 2023, vol. 24, no. 1, e215.
42. Nikolaevskii, S.A., Yambulatov, D.S., Voronina, J.K., et al., *ChemistrySelect*, 2020, vol. 5, no. 41, p. 12829.
43. Novikov, V.V. and Nelyubina, Y.V., *Russ. Chem. Rev.*, 2021, vol. 90, no. 10, p. 1330.
44. Feltham, H.L.C. and Brooker, S., *Coord. Chem. Rev.*, 2014, vol. 276, p. 1.
45. Nehrkorn, J., Valuev, I.A., Kiskin, M.A., et al., *J. Mater. Chem. C*, 2021, vol. 9, no. 30, p. 9446.
46. Matyukhina, A.K., Zorina-Tikhonova, E.N., Goloveshkin, A.S., et al., *Molecules*, 2022, vol. 27, no. 19, p. 6537.
47. Zorina-Tikhonova, E.N., Matyukhina, A.K., Chistyakov, A.S., et al., *New J. Chem.*, 2022, vol. 46, no. 44, p. 21245.
48. Yambulatov, D.S., Nikolaevskii, S.A., Shmelev, M.A., et al., *Mendeleev Commun.*, 2021, vol. 31, no. 5, p. 624.
49. Yambulatov, D.S., Nikolaevskii, S.A., Lukoyanov, A.N., et al., *New J. Chem.*, 2023, vol. 47, no. 42, p. 19362.
50. Nikolaevskii, S.A., Petrov, P.A., Sukhikh, T.S., et al., *Inorg. Chim. Acta*, 2020, vol. 508, p. 119643.
51. Yambulatov, D.S., Petrov, P.A., Nelyubina, Yu.V., et al., *Mendeleev Commun.*, 2020, vol. 30, no. 3, p. 293.
52. Petrov, P.A., Nikolaevskii, S.A., Yambulatov, D.S., et al., *Russ. J. Coord. Chem.*, 2023, vol. 49, no. 7, p. 407. https://doi.org/10.1134/S1070328423600274

53. Petrov, P.A., Nikolaevskii, S.A., Yambulatov, D.S., et al., *Russ. J. Inorg. Chem.*, 2023, vol. 68, no. 9, p. 1228. https://doi.org/10.1134/S0036023623601460
54. Petrov, P.A., Nikolaevskii, S.A., Filippova, E.A., et al., *J. Struct. Chem.*, 2024, vol. 65, no. 1, p. 117. https://doi.org/10.1134/S0022476624010116
55. Nikolaevskii, S.A. and Starikova, A.A., *J. Struct. Chem.*, 2024, vol. 65, no. 3, p. 363. https://doi.org/10.1134/S0022476624030053
56. Roy, M.M.D., Baird, S.R., Ferguson, M.J., and Rivard, E., *Mendeleev Commun.*, 2021, vol. 31, no. 2, p. 173.
57. Bantreil, X. and Nolan, S.P., *Nat. Protoc.*, 2011, vol. 6, no. 1, p. 69.
58. Efimov, N.N., Babeshkin, K.A., and Rotov, A.V., *Russ. J. Coord. Chem.*, 2024, vol. 50, no. 6, p. 363. https://doi.org/10.1134/S1070328424600141
59. *APEX3. Bruker Molecular Analysis Research Tool. Version 2018.7–2*, Madison: Bruker AXS, 2018.
60. Sheldrick, G.M., *SADABS. Bruker/Siemens Area Detector Absorption Correction Program, Version*, Madison: Bruker AXS, 2016.
61. Krause, L., Herbst-Irmer, R., Sheldrick, G.M., and Stalk, D.J., *Appl. Crystallogr.*, 2015, vol. 48, no. 1, p. 3.
62. Sheldrick, G.M., *SHELXTL. Structure Determination Software Suite. Version. 6.14*, Madison: Bruker AXS, 2003.
63. Sheldrick, G.M., *Acta Crystallogr., Sect. C: Struct. Chem.*, 2015, vol. 71, no. 1, p. 3.
64. Dolomanov, O.V., Bourhis, L.J., Gildea, R.J., et al., *J. Appl. Crystallogr.*, 2009, vol. 42, no. 2, p. 339.
65. Cirera, J., Alemany, P., and Alvarez, S., *Chem.-Eur. J.*, 2004, vol. 10, no. 1, p. 190.
66. Shang, M., Huang, J., and Lu, J., *Acta Crystallogr., Sect. C: Cryst. Struct. Commun.*, 1986, vol. 40, no. 5, p. 761.
67. Burns, J.H. and Musikas, C., *Inorg. Chem.*, 1977, vol. 16, no. 7, p. 1619.
68. Hughes, D.L. and Wingfield, J.N., *Dalton Trans.*, 1982, no. 7, p. 1239.
69. Bandoli, G. and Clemente, D.A., *J. Inorg. Nucl. Chem.*, 1981, vol. 43, no. 11, p. 2843.
70. Zalkin, A., Ruben, H., and Templeton, D.H., *Acta Crystallogr., Sect. B: Struct. Crystallogr. Cryst. Chem.*, 1982, vol. 38, no. 2, p. 610.
71. Soler, M., Mahalay, P., Wernsdorfer, W., et al., *Polyhedron*, 2021, vol. 195, p. 114968.
72. Kahn, O., *Molecular Magnetism,* Wiley-VCH, New York, 1993.
73. Rakitin, Yu.V. and Kalinnikov, V.T., *Sovremennaya Magnetokhimiya*, 1994.
74. Chilton, N.F., Anderson, R.P., Turner, L.D., et al., *J. Comput. Chem.*, 2013, vol. 34, no. 13, p. 1164.

Translated by E. Yablonskaya